



## Modeling and Analysis of Thermal Pipe by Matlab to Greenhouse Heating

**Jihad Kadhim AbdAli<sup>1</sup>**

Ph.D.Power.Mech.Engg  
Field Crops, Agricultural College, Al.Qasim Green University, Babil,  
Iraq  
Email: [jihadhpvit@gmail.com](mailto:jihadhpvit@gmail.com)

**Maysoon Khazaal Abbas  
Maarroof<sup>1</sup>**

Msc. Information Technology.  
Basic Education College,  
University of Babylon, Babil, Iraq  
Email: [maysoonalmarroof@gmail.com](mailto:maysoonalmarroof@gmail.com)

### ABSTRACT

In the present work a thermal pipe is modelled, designed by matlab program 8.5 in order to use a heating mechanism through night or cloudy days in the cold climate. Heat transfer as geothermal energy from underground to the environment inside the greenhouse without loss any type of energy consumption but energy conservation. This technique is one of the latest applications of the heat transfer devices to transfer heat and energy. The heat transfer device is made of a sealed copper metal tube containing graphene oxide nanofluid as operation fluid. It is divided into three parts; the evaporator, adiabatic and condenser section. The active part of thermal device is the evaporator reign which transfers heat from the underground to the working fluid, which is in turn, transfers energy to the condenser part where it is dissipated to the surrounding of the greenhouse. This study was conducted on a greenhouse with an area of (12) m<sup>2</sup>. Mathematical model construct by applying the explicit technique when used the convergent values. Results show the heat transfer rates are increase, with stability, the environment temperature of the greenhouse when thermal heat transfer device is executed in the cold and cloudy period of the cold time. The temperature inside the greenhouse reached (25) °C when thermal device inserted inside the soil to a level of (2.5) m with heat transfer rate of (500) W, while the outside temperature was about (15) °C.

### Keywords:

heat transfer device, greenhouse and heating, nanofluid.

### Introduction

Greenhouse mostly used in fall and cold months when temperature level of environment is drop. When the temperature decreases below 14 °C it may be cause damage to the plants. In order to increase the temperature indoor, in that types of greenhouse plants heat transfer device can be used to increase the temperature of greenhouse surrounding. In the cold days that

which possible to grow the plants in greenhouses without consuming the electric energy. Heat transfer device is highly efficient heat transfer depending upon the transfer the energy by small surface area and very little losses with small temperature difference, which use the continuous evaporation and condensation of a suitable working fluid. Since

the latent heat of vaporization for working fluid when it's selected is very large.

Investigation of an instrumented thermal pipe for domestic heating that uses water as a working fluid was carried out by (AL-Saadi, 2005). Heat transfer device appliance can be seen in science industry and daily life as cooler or heat transport device between two environments with different temperatures. Theoretically heat transfer device can be transfer high amount of energy with temperature difference of 10°C. Useful output of this device is about 98%-99% (Reay, 2006). Due to a variety of advantage features, thermal devices have been used in a number of applications, both in space and terrestrial technologies. Some applications of thermal pipes are in cooling electronic devices and heat recovery from exhaust ventilation (Shunji and Suzuki;(2000)). In this work the device is used to heat the greenhouse by using the temperature of inside the underground as a heat

source. It's inserted into the soil at the definite levels.

### 1. Thermal device components.

As shown schematically in Figure (1), Thermal device consists of a galvanized pipe by a diameter ( $d_i=70\text{mm}, d_o=76\text{ mm}$ ) and (50cm) length of evaporator and (75cm) length of condenser and rectangular finned putted radially upon the dissipation part in order to increase the heat rejects and energy to the environment by natural convection.. The passing of vapor from evaporator to condenser will be through the adiabatic section. The nanofluid was used as working fluid in this device. Wick section is the groove made from copper was inserted along the inside surface of the device. The fins were welded to the outside surface of the condenser. Galvanized copper was chosen because of its good heat transfer properties and thermal conductivity. The device was cleaned, sealed and evacuated to be prepared for use.

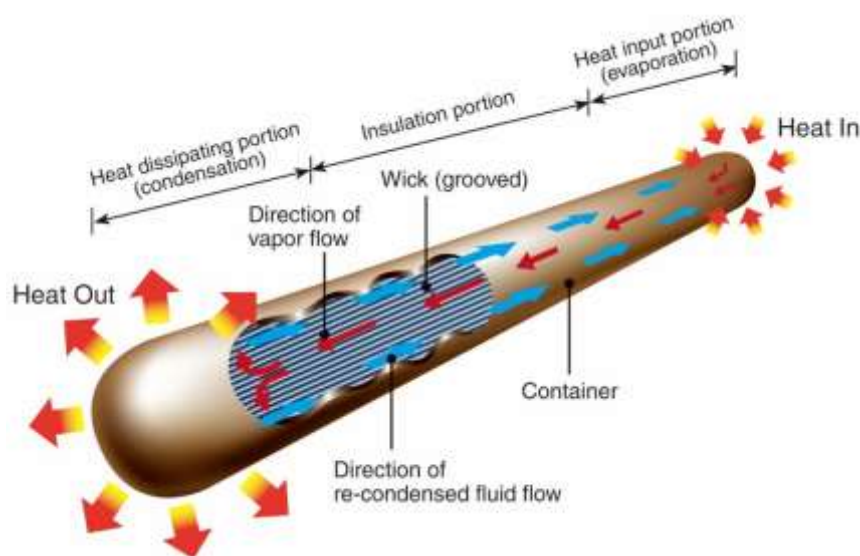


Figure (1) heat transfer device components,[5].

### 2. Temperature Measurements

24 calibrated thermocouples type k were used in temperature measurement, ten on the evaporator section, two thermocouples

distributed along the adiabatic part and 12 upon condenser section. The temperature in the surrounding inside the greenhouse was measured directly from a digital display device.

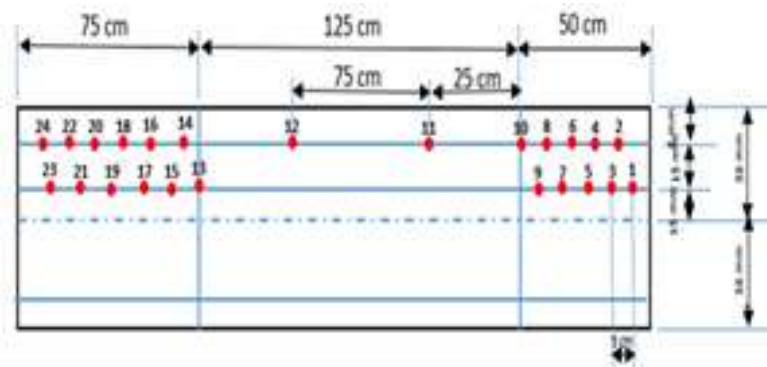


Figure (2) distribution of thermocouples on thermal device

**3. Greenhouse characteristics**

In this work the greenhouse used is composed of metal frame covered by a plastic shell. It is destined for growing variant types of plants. It had dimension, length=4m; width=3m and height=2.25m, an area of 12 m<sup>2</sup>.

**4. Theoretical Model of Thermal device**

A theoretical unsteady state model describing the performance of the heat transfer device under a variety of operating conditions is developed below:

**4.1. Evaporation part**

The energy equation can be apply as follows:

$$\frac{1}{\alpha} \frac{\partial T}{\partial t} + \frac{v_l}{\alpha_l} \frac{\partial T}{\partial z} = \frac{\partial^2 T}{\partial r^2} + \frac{1}{r} \frac{\partial T}{\partial r} + \frac{1}{r^2} \frac{\partial^2 T}{\partial \theta^2} + \frac{\partial^2 T}{\partial z^2} \quad (1)$$

when  $\alpha = \frac{k}{\rho c_p}$ .

All of the focuses have domain-limit dimensions. It has been assumed that a half-domain of the cylinder has been used to design the model because of its symmetrical shape. Numerical simulations have been performed using an explicit technique.

$$\frac{T_{i+1,j}^n - 2T_{i,j}^n + T_{i-1,j}^n}{\Delta r^2} + \frac{1}{r_i} \frac{T_{i+1,j}^n - T_{i-1,j}^n}{2\Delta r} + \frac{T_{i,j+1}^n - 2T_{i,j}^n + T_{i,j-1}^n}{\Delta z^2} = \frac{1}{\alpha} \frac{T_{i,j}^{n+1} - T_{i,j}^n}{\Delta t} + \frac{v_l}{\alpha_l} \frac{T_{i,j+1}^n - T_{i,j-1}^n}{2\Delta z} \quad (2)$$

The boundary conditions are at z=0 and r=R,  $-k \frac{\partial T}{\partial r} = \bar{q}$  (heat flux) at z=50, T=T<sub>v</sub>

**4.1.1 Temperature through the liquid phase**

In the liquid phase, a two-dimensional transient energy equation with polar coordinates allows the temperature distribution in an interface region of limited space to be determined before a change of phase occurs on an interface line, as shown in Figure 3. The interface line is located 35 cm from the left side of the evaporator. The liquid temperature was increased to a saturated temperature (boiling point) at the interface line; this records the vaporisation process. At this time, the remaining fluid has stagnated and its velocity is equal to zero. The computer program, depending on the boundary conditions, has a greater capacity to measure temperature profiles through the r and z plane when the explicit scheme is applied.

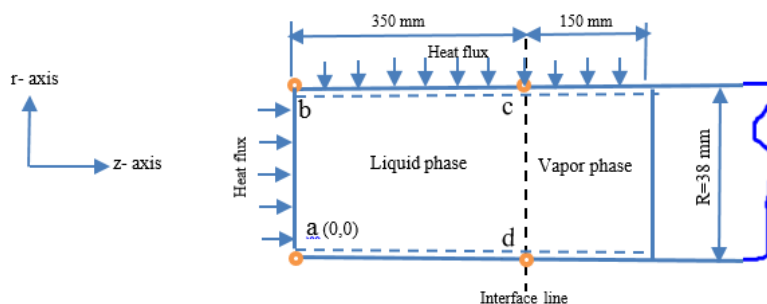


Figure (3) Evaporator dimensions and boundary condition on it

## 1. Temperature at Point a

Point a represents the starting location of the liquid phase in the evaporator. At this point, r and z coordinates are 0, 0, where r=0 and z=0 after applying the energy balance to this boundary node, which is a corner node.

$$T_{i,j}^{n+1} = 4\lambda_1 T_{i+1,j}^n + (1 - 6\lambda_1)T_{i,j}^n + 2\lambda_1 T_{i,j+1}^n - 2 \frac{\lambda_1 q^- \Delta r}{K} \quad (3)$$

where  $\lambda = \frac{\alpha_i \Delta t}{\Delta r^2} \leq 0.5$  is the Fourier number and  $\lambda_1 = \frac{\alpha_i \Delta t}{r_i \Delta r}$ .

## 2. Temperature distribution through the r-axis

To find the temperature through the r-axis in the liquid phase, an energy balance on the boundary line was applied. For r>0 and z=0, the explicit scheme was constructed as:

$$T_{i,j}^{n+1} = \lambda T_{i+1,j}^n + \lambda T_{i-1,j}^n + (1 - 4\lambda_1)T_{i,j}^n + 2\lambda_1 T_{i,j+1}^n - \frac{2\lambda q^- \Delta r}{K} \quad (4)$$

### 1. Temperature distribution at corner point b

The energy balance was applied for this boundary node, and the temperature was estimated as:

$$T_{i,j}^{n+1} = 2\lambda T_{i,j+1}^n + (1 - 4\lambda)T_{i,j}^n + 2\lambda T_{i-1,j}^n - 4 \frac{\lambda q^- \Delta r}{K} \quad (5)$$

### 2. Temperature distribution through line bc in the liquid phase

This is also a boundary line; therefore, the energy balance was needed. Temperature distribution was obtained when r=R and z>0, i.e. i=R to R and j=0 to 349.

$$T_{i,j}^{n+1} = 2\lambda T_{i-1,j}^n + (1 - 4\lambda)T_{i,j}^n + \lambda T_{i,j+1}^n + \lambda T_{i,j-1}^n - 2 \frac{\lambda q^- \Delta r}{K} \quad (6)$$

### 3. Temperature distribution through the z-axis in the liquid phase

The temperature was calculated by applying the two dimensions of the energy equation when r=0 and z>0, i.e. i=1 to 1, j=2 to 349 and  $T_{i+1,j} = T_{i-1,j}$ .

$$T_{i,j}^{n+1} = 4\lambda T_{i+1,j}^n + (1 - 6\lambda)T_{i,j}^n + \lambda T_{i,j+1}^n + \lambda T_{i,j-1}^n \quad (7)$$

### 4. Temperature distribution through the r-z plane in the liquid phase

The temperature was calculated by applying the two dimensions of the energy equation where r>0, i=1 to L-1, z>0 and j=2 to 349.

$$T_{i,j}^{n+1} = (\lambda + \frac{\lambda_1}{2})T_{i+1,j}^n + (1 - 4\lambda)T_{i,j}^n + (\lambda - \frac{\lambda_1}{2})T_{i-1,j}^n + \lambda T_{i,j+1}^n + \lambda T_{i,j-1}^n \quad (8)$$

#### 4.1.2 Temperature distribution through the vapour phase in the evaporator

##### 1. Temperature distribution through the z-axis

At the z-axis where z>350, r=0 and  $c = \frac{\Delta t v_a}{\Delta z}$  is the Courant number  $0 \leq c \leq 1$ .

the following energy equation should be used:

$$T_{i,j}^{n+1} = 4\lambda T_{i+1,j}^n + (1 - 6\lambda)T_{i,j}^n + (\lambda - \frac{c}{2})T_{i,j+1}^n + (\lambda + \frac{c}{2})T_{i,j-1}^n \quad (9)$$

##### 2. Temperature distribution in the r-z plane in the vapour phase

$$T_{i,j}^{n+1} = (\lambda + \frac{\lambda_1}{2})T_{i+1,j}^n + (1 - 4\lambda_3)T_{i,j}^n + (\lambda - \frac{\lambda_1}{2})T_{i-1,j}^n + (\lambda - \frac{c}{2})T_{i,j+1}^n + (\lambda + \frac{c}{2})T_{i,j-1}^n$$

(10)

#### 4.2. Adiabatic Section

The adiabatic section was designed using suitable dimensions, materials and insulation properties so that the heat transfer device would work as a cooling device. The working fluid vapour was passed through this section with no loss of temperature. The vapour temperature of the working fluid was considered the initial value of the temperature in the condenser section because there was no heat transfer between the system and its surroundings in the adiabatic section when it

was insulated by a layer of glass wool. The phase change phenomenon did not occur in this section.

#### 4.3. Condenser section

The working fluid entered the condenser section as a vapour for 120 min. The vapour changed to liquid at the interface line and phase change occurred at 45 cm from the z-axis. Heat was rejected by the high-fins that were specifically designed for this section. The liquid phase continued to the last node of the

condenser's dimensions. The energy equation was applied to predict the temperature distribution for the condenser section in two

zones (vapour-liquid), as shown in figure (4).

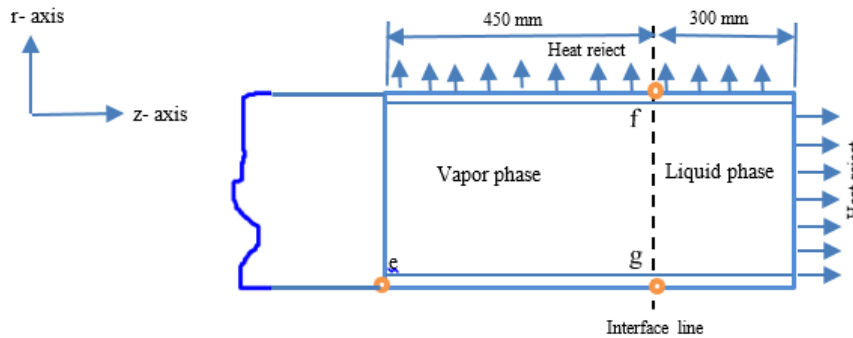


Figure (4) Condenser dimensions.

### 4.3.1 Temperature distribution through the vapour phase in the condenser

The domain area of the vapour phase and the interface line was evaluated at 45 cm from the left, as illustrated in Figure 3. The initial temperature in the condenser was the vapour temperature when it left the evaporator after two hours in the device.

#### 1. Temperature distribution through the z-axis

Where  $r=0$  and  $z>0$ , i.e.  $i=1$  to 1 and  $j=0$  to 449, then the energy equation was used. The equation was represented with an explicit technique when  $r=0$  as :

$$T_{i,j}^{n+1} = 4\lambda T_{i+1,j}^n + (1 - 6\lambda)T_{i,j}^n + (\lambda - \frac{c}{2})T_{i,j+1}^n + (\lambda + \frac{c}{2})T_{i,j-1}^n \quad (11)$$

#### 2. Temperature distribution through the r-z plane in the vapour phase

Temperatures of the vapour phase in the r-z plane were calculated at  $r>0$  and  $z>0$ , i.e.  $i=2$  to L-1 and  $j=2$  to 449. The energy equation was used to estimate the temperatures through the r-z plane:

$$T_{i,j}^{n+1} = (\lambda + \frac{\lambda_1}{2})T_{i+1,j}^n + (\lambda - \frac{\lambda_1}{2})T_{i-1,j}^n + (1 - 4\lambda_3)T_{i,j}^n + (\lambda - \frac{c}{2})T_{i,j+1}^n + (\lambda + \frac{c}{2})T_{i,j-1}^n \quad (12)$$

### 4.3.2 Temperature distribution through the liquid phase in the condenser

It was assumed that the vapour would change to liquid after interface line gf. Then, the temperature distribution of the liquid domain in the condenser was simulated using the energy equation.

#### 1. Temperature distribution through the z-axis in the liquid phase

When  $r = 0, z>0$ , i.e.  $i=1$  to 1,  $j=451$  to m-1 and  $c_1 = \frac{v_*\Delta t}{\Delta z}$ , the energy equation was presented explicitly as:

$$T_{i,j}^{n+1} = 4\lambda T_{i+1,j}^n + (1 - 6\lambda)T_{i,j}^n + (\lambda - \frac{c_1}{2})T_{i,j+1}^n + (\lambda + \frac{c_1}{2})T_{i,j-1}^n \quad (13)$$

#### 2. Temperature distribution through the r-z plane in the liquid phase

When  $r>0$  and  $z>0$ , i.e.  $i=2$  to L-1 and  $j=451$  to m-1, the energy equation was formed explicitly as:

$$T_{i,j}^{n+1} = (\lambda + \frac{\lambda_1}{2})T_{i+1,j}^n + (1 - 4\lambda)T_{i,j}^n + (\lambda - \frac{\lambda_1}{2})T_{i-1,j}^n + (\lambda - \frac{c_1}{2})T_{i,j+1}^n + (\lambda + \frac{c_1}{2})T_{i,j-1}^n \quad (14)$$

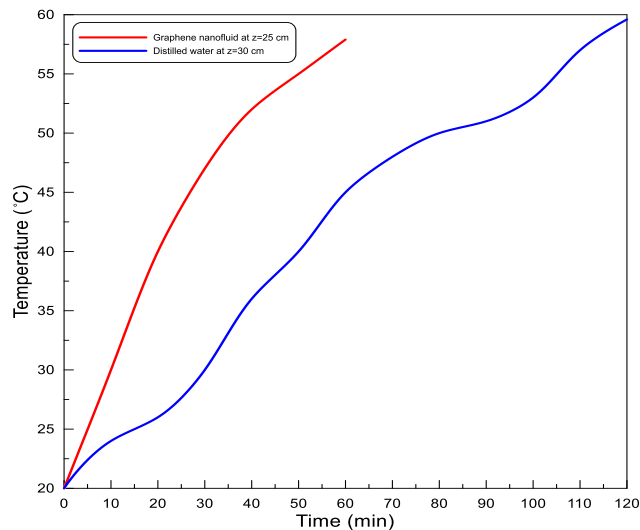
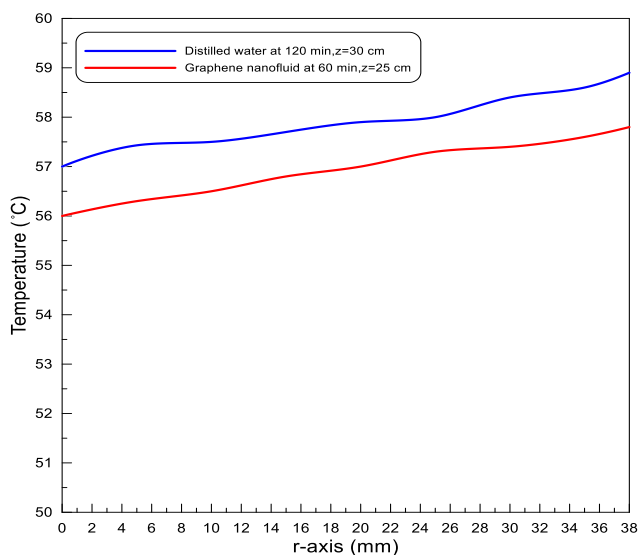
## 5. Results and discussion

Theoretical results these relate the basic parameters of the thermal pipe, average temperatures of the evaporator and condenser sections, under various operating conditions are presented and discussed along with performance indices represented by the heat

transfer rate of the heat transfer device that calculated 500 W and its efficiency. The results show that the temperature inside the greenhouse remains within the acceptable required temperature for plant growth. The results and relevant discussion are given as follow:

The temperature distribution in liquid phase of evaporator part was illustrated in figure (5), when the water was working fluid the temperature of it was started from 57 to 59 °C after 120 minute of the operation time interval, all evaluated values of temperature with respect to radius values of pipe. Nanofluid was enhanced the heat transfer rate and temperature distribution was different about the distilled water, the values of temperature

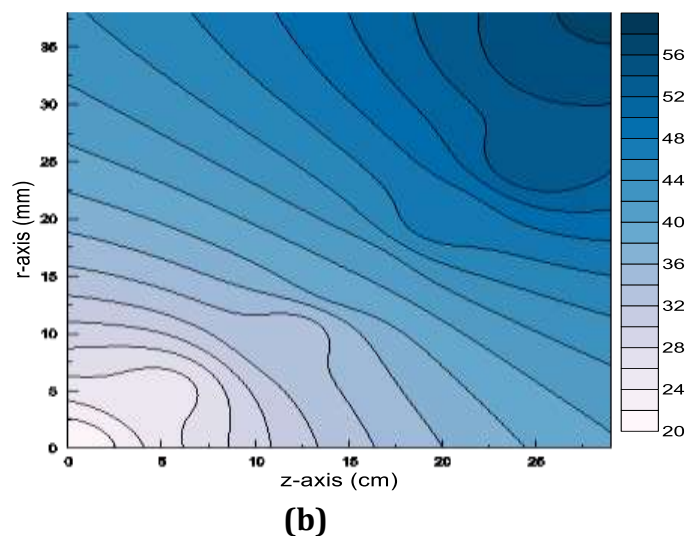
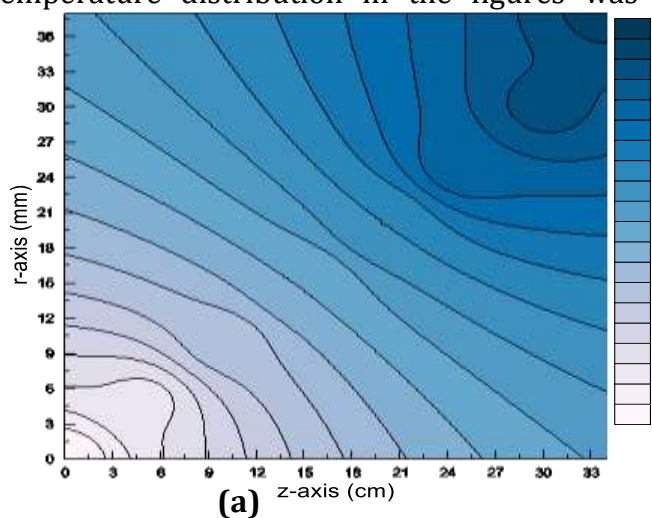
range decreased to started from 56 to 58 °C. In figure (6) the temporal variation in temperature with different periods of time in liquid phase at value of  $r = 0$ , temperature of nanofluid working fluid was increased with time but the distilled water was less than nanofluid temperature because of the graphene nanoparticles have high thermal conductivity and it have more ability to enhance the heat transfer rates.



**Figure (5)** temperature distribution of liquid phase with different value of r axis. **Figure (6)** temporal variation of liquid phase at different time intervals

Figure (7) explains isothermal contour of temperature distribution through (r-z) plane in liquid phase at time 120 min for distilled water, and for nanofluid at time 60 min. The temperature distribution in the figures was

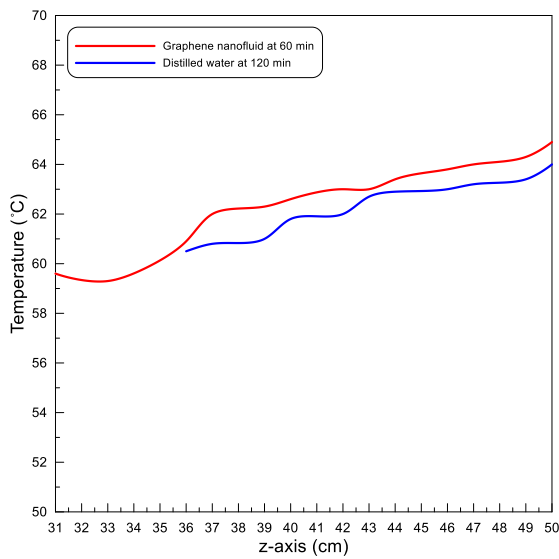
evaluated from 20 to 58 °C, different values of temperature inside the contours and the time was different to reach the temperature range in this period



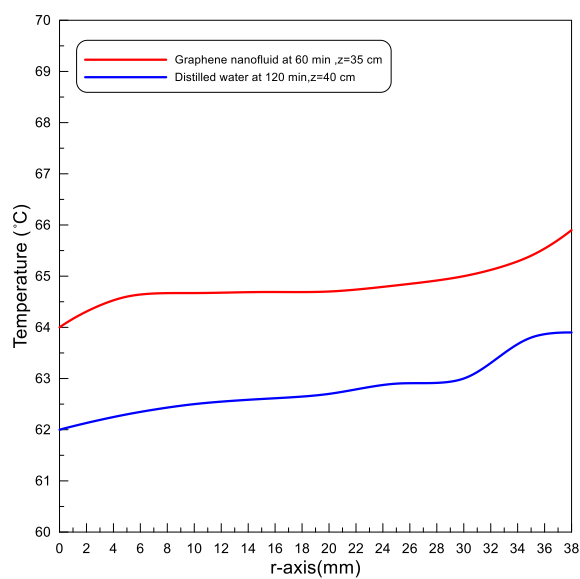
**Figure (7)** a-isothermal contour of temperature distribution through (r-z) plane in liquid phase at time 120 min for distilled water, b- at time 60 min. for nanofluid.

Figure (8) illustrates the temperature distribution of vapor phase through z-axis,  $r = 0$ , the temperature values of the nanofluid was increased with increased the z- axis values and started from 58 to 86 °C, for nanofluid and started from 60 to 83 °C when using the distilled water. Figure (9) shows the temperature distribution of vapor phase in evaporator section at different time intervals with different values of radius. The temperature values of nanofluid particles have more energy and heat if we compared with distilled water. Figure (10)

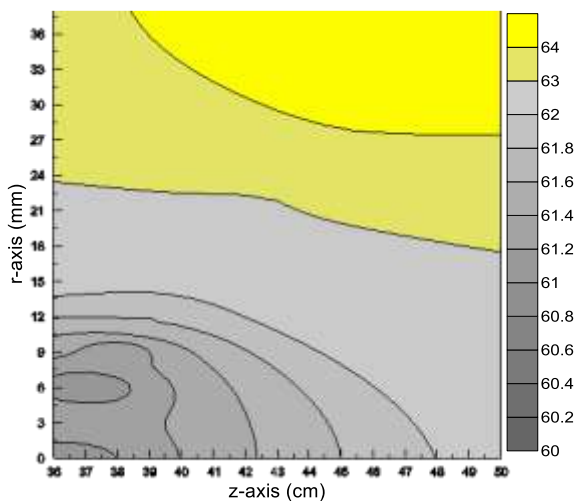
demonstrate isothermal contour map of temperature distribution through vapor phase at time = 120 min for distilled water in evaporator section, while time = 60 min for nanofluid. The two ours of time was represented the time of phase change phenomena for working fluid inside thermal device when the liquid convert to vapor by increasing of energy and heat if the distilled water was used. When the graphene oxide nanofluid the time of phase change was one hour.



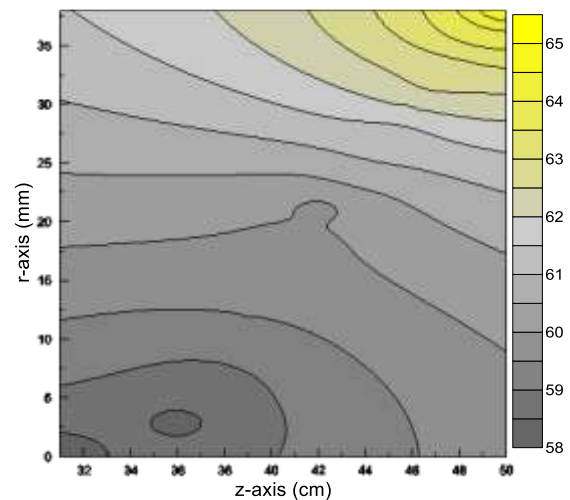
**Figure (8)** temperature distribution of phase through z-axis,  $r = 0$



**Figure (9)** temperature distribution of vapor phase at different time intervals.



**(a)**



**(b)**

**Figure (10)**a- isothermal contour map of temperature distribution through vapor phase at time = 120 min for distilled water, b- at time = 60 min for nanofluid.

Figure (11) explains the temperature distribution of vapor phase when revalue equal to zero and phase change location was different in condenser section with value of r-axis. The temperature was observed decreased in this part because of the heat and energy would be dissipated to the environment by more surface area of fins. Figure (12) illustrates the temporal variation in temperature at different time in condenser section, when time period was equal to 140 minute its mean the time of phase change occurrence in the condenser part for distilled water .90 minute time of phase change for nanofluid. Figure (13) shows isothermal

contour of temperature distribution through (r-z) plane in vapor phase at time 140 min. for distilled water in condenser section and at 90 min. for nanofluid. All temperature values were decreased in this part. The temperature values were continued decrease even the phase change phenomenon was happened to convert the vapor of working fluid to liquid as shown in figure (14) the isothermal contour map of temperature distribution through liquid phase at time = 140 min for distilled water, b- 90 min for nanofluid. When the vapor lost the high energy it would be convert to low level as liquid phase.

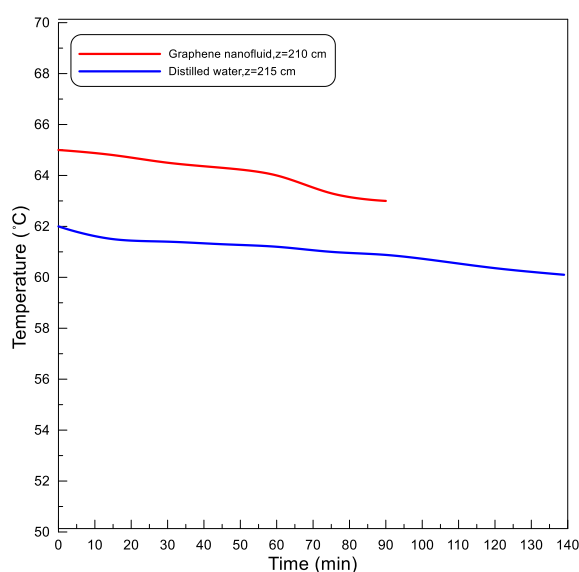
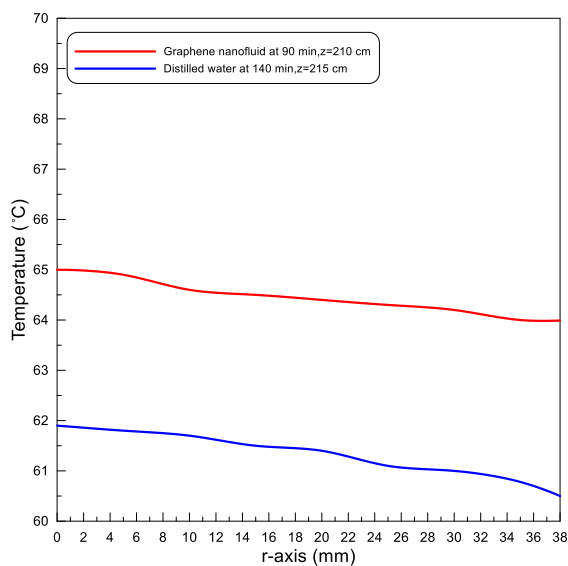
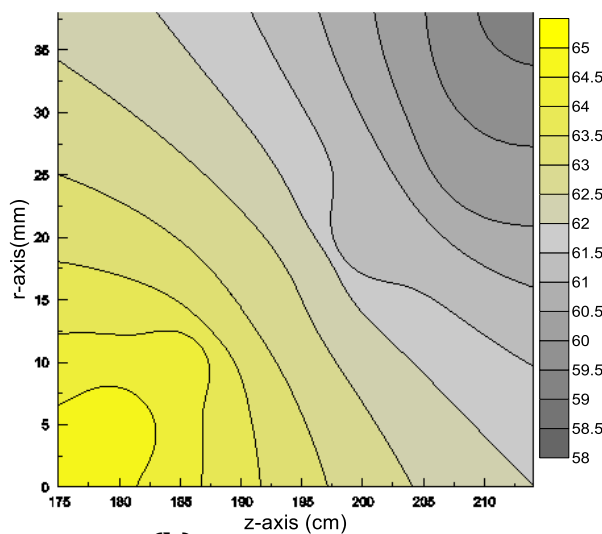
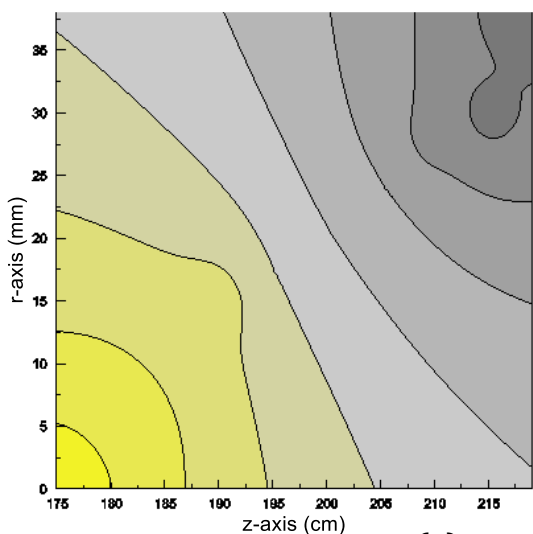


**Figure (11)** temperature distribution of vapor phase temperature in the condenser section.

**Figure (12)** temporal variation in at different time in condenser section



(a)

(b)

**Figure (13)**a- isothermal contour of temperature distribution through (r-z) plane in vapor phase at time 140 min. for distilled water,b- at time 90 min. for nanofluid.

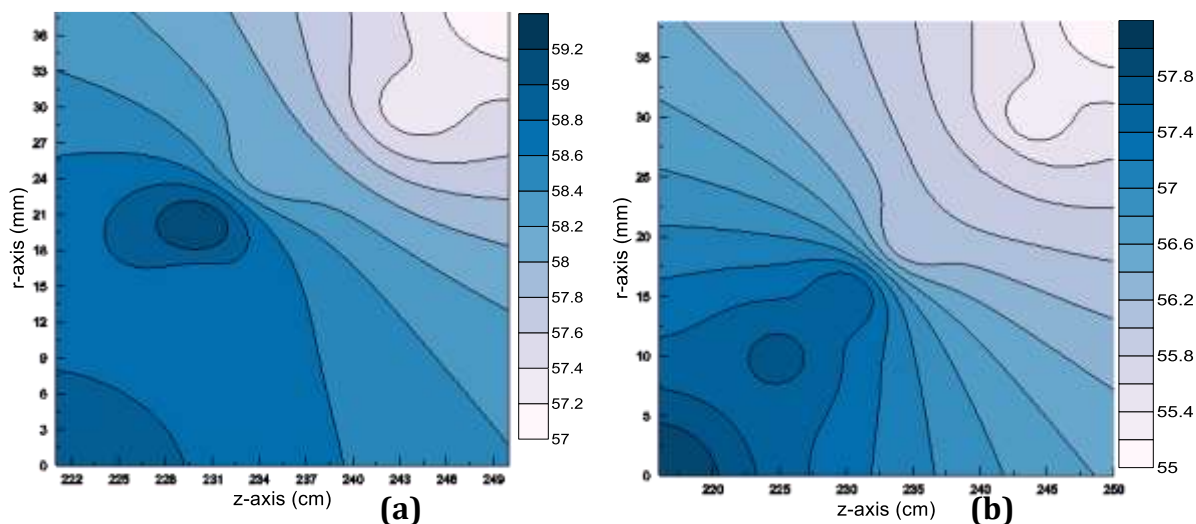


**Figure (14)** a- isothermal contour map of temperature distribution through liquid phase at time = 140 min for distilled water, b- at time = 90 min for nanofluid.

Figure (15) denote to comparison between the theoretical results of present work and another study for temperature distribution through thermal device along the device length. The

temperature value of present work was more increased and acceptance if compared with another model.

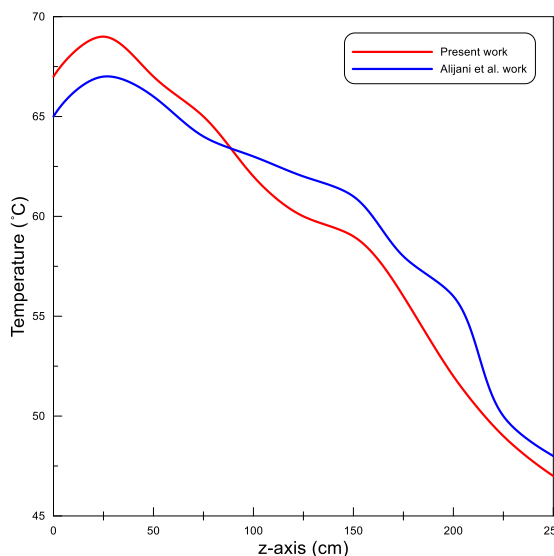


**Figure (15)** comparison between the theoretical results of present work and another study for temperature distribution through thermal device.

### 6. Conclusions

From the present work, the following conclusions can be obtained:

1. A mathematical model was predicted for the direct simulation of time-dependent phase process is solving the evaporation and condensation processes, and the

temperatures distribution through the thermal device. This depending upon many assumptions for each phase and the moving boundary condition inside domain (interface). Thermo-physical properties of each phase remain uniform and constant.

2. Thermal efficiency was improved to 15 % by using nanofluid. This is due the duration time of evaporation and condensation processes were decreased in heat transfer device.
3. Graphene oxide nanoparticles were adding by weight fraction concentrations (0.075) consider stable, deposition of it upon the wall of wick in the evaporator section was enhanced the capillary property in this part.
4. Using thermal pipes in greenhouses as a device to exploited effectively geothermal energy in heating during night or cloudy days in the cold months.
5. The maximum efficiency of the thermal pipe obtained when it is buried to depth of (3.5)m and the filling ratio is (30%) to achieve surrounding temperature inside the greenhouse (20)°C which is convenient to plant growth.
6. Thermal device efficiency increases with the increase of the depth to which the pipe buried inside the soil.
7. The initial and running cost of such project is low compared with the conventional heating methods.
8. Design of system are simple with very low maintenance because there are no rotating parts. In addition, the heat transfer device pipe can be used as supporting frame for the greenhouse.

## 7. Nomenclature

1.  $c_{pL}$  Specific heat capacity of liquid at constant pressure J/kg.k
2.  $c_{pV}$  Specific heat capacity of vapour at constant pressure J/kg.k
3.  $k_L$  Thermal conductivity of liquid phase W/m.k
4.  $k_V$  Thermal conductivity of vapour phase W/m.k
5.  $k_{nf}$  Thermal conductivity of nanofluid W/m.k
6.  $k_{bf}$  Thermal conductivity of base fluid W/m.k
7.  $V_a, V^*$  Velocities of interface m/s
8.  $T$  Temperature k
9.  $t$  Time s
10.  $\rho$  Density kg/m<sup>3</sup>
11.  $\alpha_L$  Thermal diffusivity of liquid phase m<sup>2</sup>/s
12.  $\alpha_V$  Thermal diffusivity of vapour phase m<sup>2</sup>/s
13.  $\rho_L$  Density of liquid phase kg/m<sup>3</sup>

14.  $\rho_V$  Density of vapour phase kg/m<sup>3</sup>
15.  $\delta(t)$  Location of liquid-vapour interface m
16.  $\Delta r$  Increment distance through r-axis mm
17.  $\Delta z$  Increment distance through z-axis cm
18.  $\lambda_{1,2,3,4}$  Convergent

## References

1. AL-Saadi, Z. 2005. Design and Implementing a Heat Pipe Experimental System for Residential Heating. M. Sc. Dissertation, Baghdad University, College of Engineering.
2. Bejan, A. and Kraus A.D. 2003. Heat Transfer Handbook. Published by John Wiley & Sons, Inc., Hoboken, New Jersey.
3. El-Wakil M. M. 1988. Nuclear Power Engineering. 8th ed., Me Graw-Hill Book Company.
4. Kreith,F.,Boehm,R.F.,Raithby,G.D. and Hollands,K.G. 2000.Heat and Mass Transfer Handbook. CRC Press LLC.
5. Reay, D.A. and Kew,p. (2006). Heat Pipes Theory, Design and Applications. 5rd. Edition, Britain.
6. Shunji, K. and H. Suzuki 2000 Proceedings World Geothermal Congress, Kyushu-Tohoku.
7. Zhao S, Xu G, Wang N and Zhang X 2018 *Nanomaterials*. **8(2)** 6–16
8. Muhieddine M and Canot EMarch R 2018 *International Journal on Finite Volumes*. **6(1)** 1–19
9. Alijani H, Cetin B, Akkus Y and Dursunkaya Z 2017 ICCHM<sup>2</sup>T2017May 28–June 1.**160221** 1–9
10. AbdAli J, Alwan A and Hameed R 2019 *Test Engineering and Management*. **83(3)** 13182–13198.
11. AbdAli J, Alwan A 2020 IOP Conf. Series: Materials Science and Engineering **987** 012017.